What makes a flare?

Determining the Photospheric Magnetic Signature of a Flaring Active Region

K. D. Leka

Colorado Research Associates Div.,
NorthWest Research Associates, Inc.

With: **Graham Barnes**, *CoRA/NWRA*
Don Mickey, *U. Hawai'i*
Barry LaBonte, *JHUAPL*
Mees Solar Observatory Observing Staff

- Using photospheric magnetic field data to predict solar flares
- Imaging Vector Magnetograph data
- Is there anything there?
- The statistical tests
- Measuring coronal complexity

This work was carried out at the Colorado Research Associates Division of NorthWest Research Associates, Inc., with data from the U. Hawai`i Mees Solar Observatory. Funding from the Air Force Office of Scientific Research is gratefully acknowledged under contracts F49620-00-C-0004, F49620-03-C-0019 and F49620-02-C-0191.

Q: Can we tell which active region will flare?

"Observer's wisdom":

Active regions which are *large, complex,* and *evolving* have a greater likelihood of producing a solar flare.

- Energetic events are usually associated with larger active regions; more area, more magnetic flux implies greater energy storage.

- The more magnetically complex a region is, the more it deviates from the lowest-energy state (and the more energy is available to be released in a flare). Active regions in the "δ" configuration are extreme examples of this.

- Evolving active regions, especially with new emerging magnetic flux, bring additional magnetic energy to the system and increase the magnetic complexity and energy available for flares.

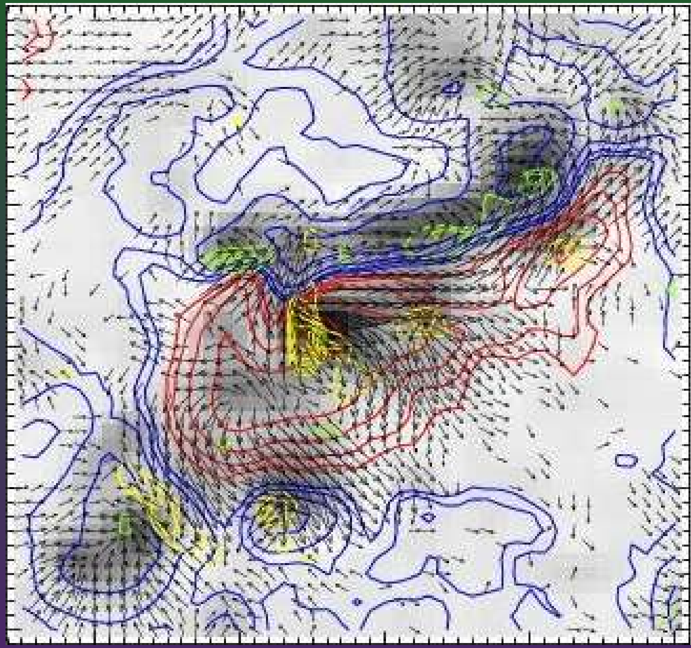

Q: Can we tell *when* an active region is going to flare?

***If* the energy for solar flares is stored in, and released from, the magnetic field, that process *should* be observable in the active region's magnetic field configuration.**

[the "*stress&release*" picture for solar flare energy]

- The photosphere provides the boundary condition for upper atmospheric layers; measuring the photospheric magnetic field should indicate the energy storage in the active region.

- Numerous measures of magnetic energy storage and complexity can be derived from the photospheric field.

- Prior work examining the correlation of these measures to solar flare activity have provided *initial evaluations* of those measures.

- Many examples have been published showing changes in photospheric fields *associated with* solar flares, *c.f.* recent observations by Wang *et al.*

- We propose here a next step....

Imaging Vector Magnetograph, Mees Solar Observatory

- Telecentric design with near-normal reflections for minimal instrumental polarization
- Helium-filled telescope and image stabilizer minimize seeing-induced polarization
- Fabry-Perot-based imaging system provides large (280"x280") Field-of-View
- Spectral line sampled 20-40 times across line of choice (Photosphere: 630.25nm, others available)
- Liquid-Crystal modulators plus a 4-step modulation scheme provide fast polarization sampling.
- Full Stokes spectra dataset in less than 2 minutes.

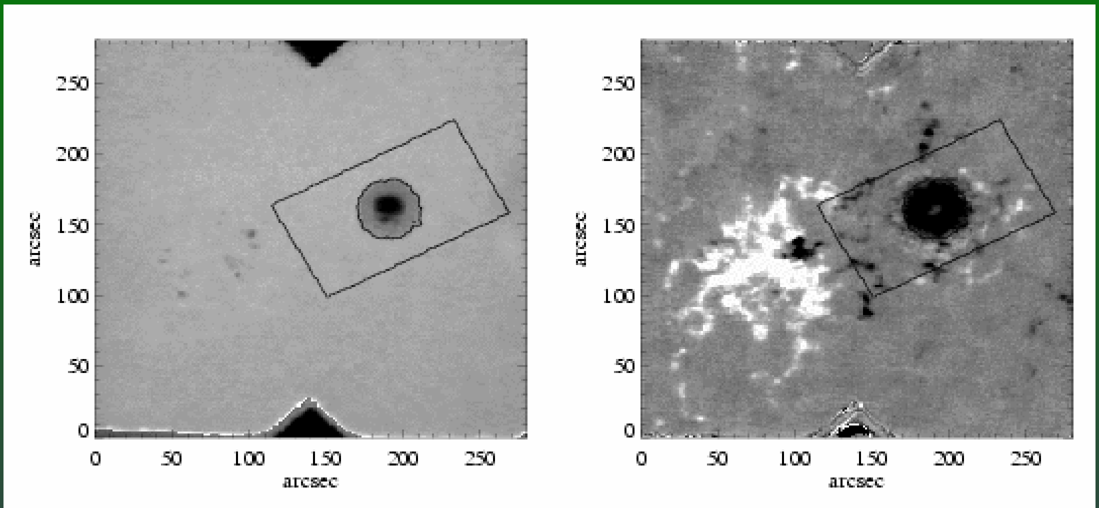

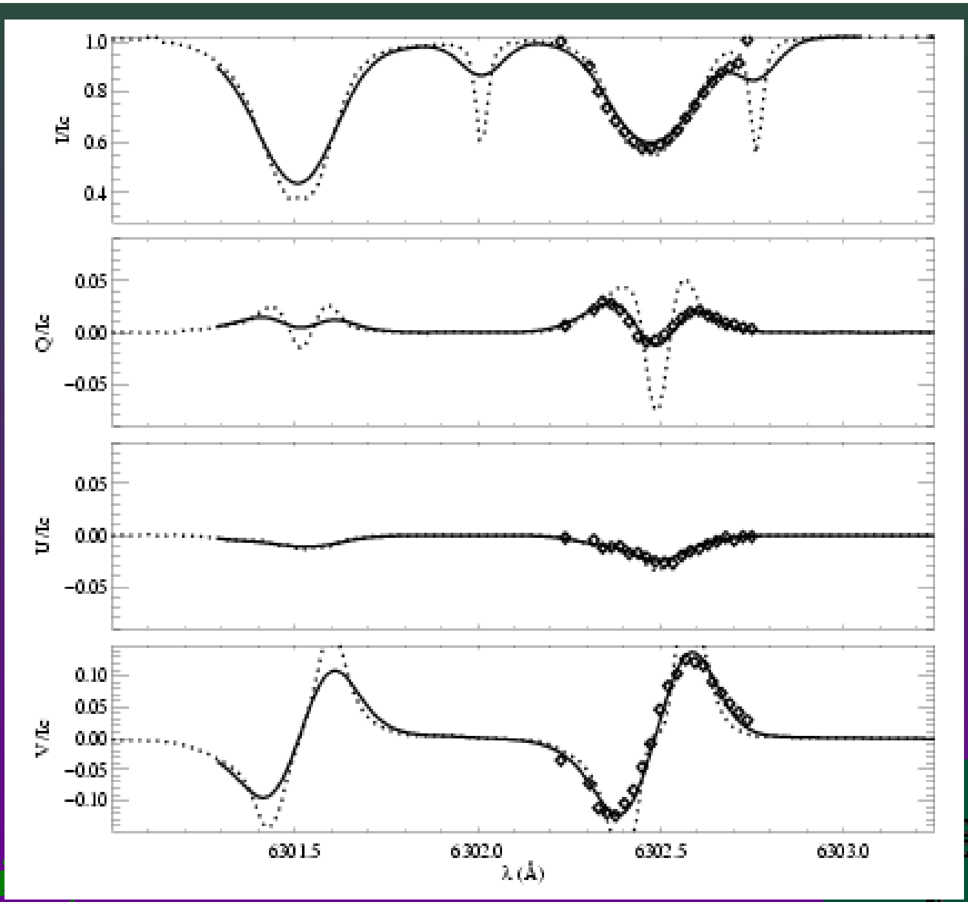

Polarization Spectra into Magnetic Field Maps

➢Radiative-Transfer based inversion procedure to obtain ***B, f***, *etc*.

➢Transform observed [*Bl, Bt,* ϕ] components to heliographic [*Bx, By, Bz*]

➢ Iterative approach to ambiguity resolution, with additional constraint for consistency in time-series data.

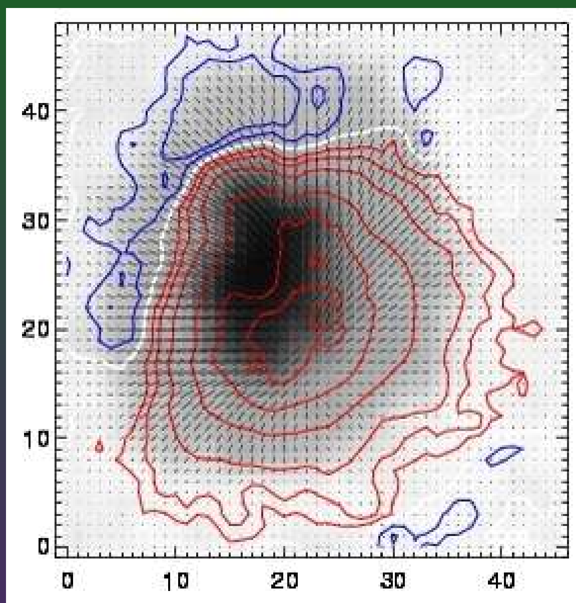

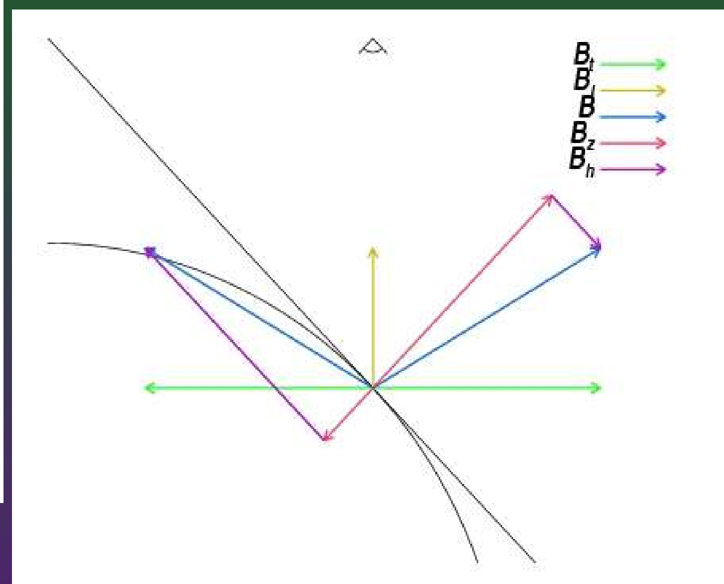

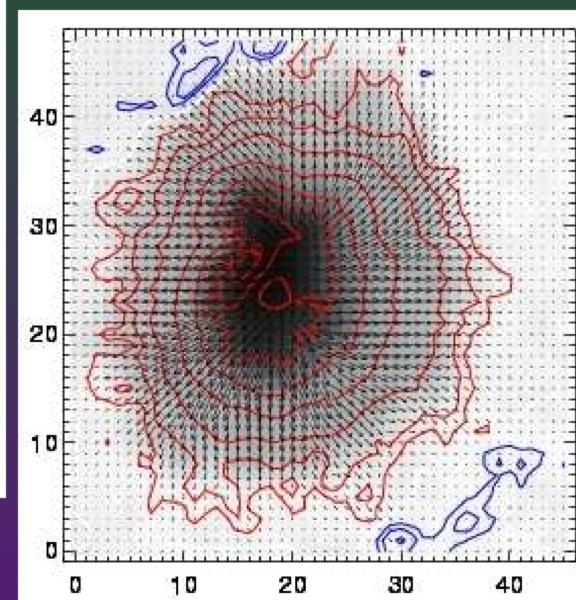

➢Full consideration of both random and systemmatic uncertainties: effects of atmospheric seeing is explicitly modeled and included as an additional source of uncertainty (*cf* Leka & Rangarajan, 2001).

Accounting for the effects of variable atmospheric seeing:

- A significant effect which must be accounted for in all ground-based time-series data
- For imaging systems, one can model and account for the effects
- [For spectrograph-based systems, seeing varies temporally (thus spatially), and so is difficult to model].

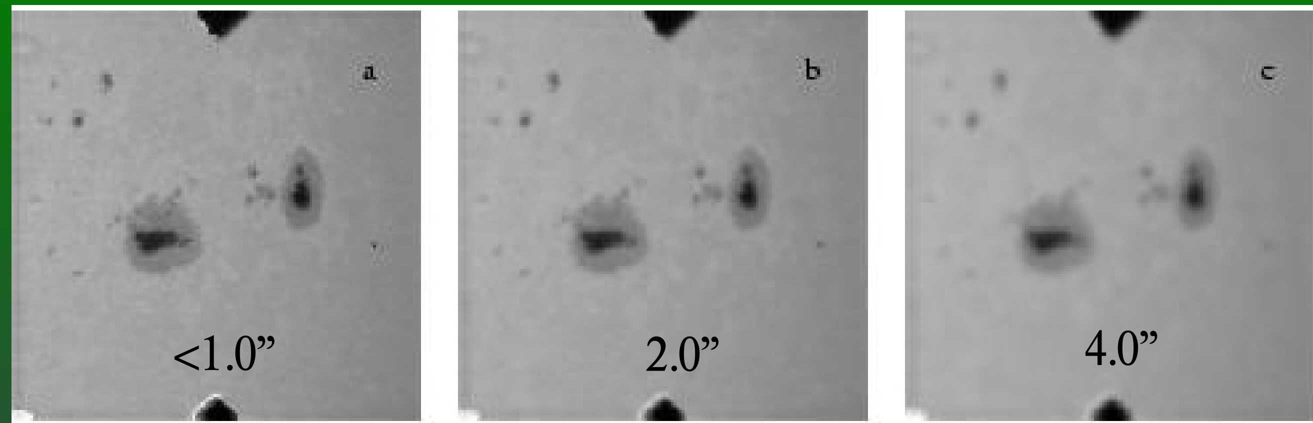

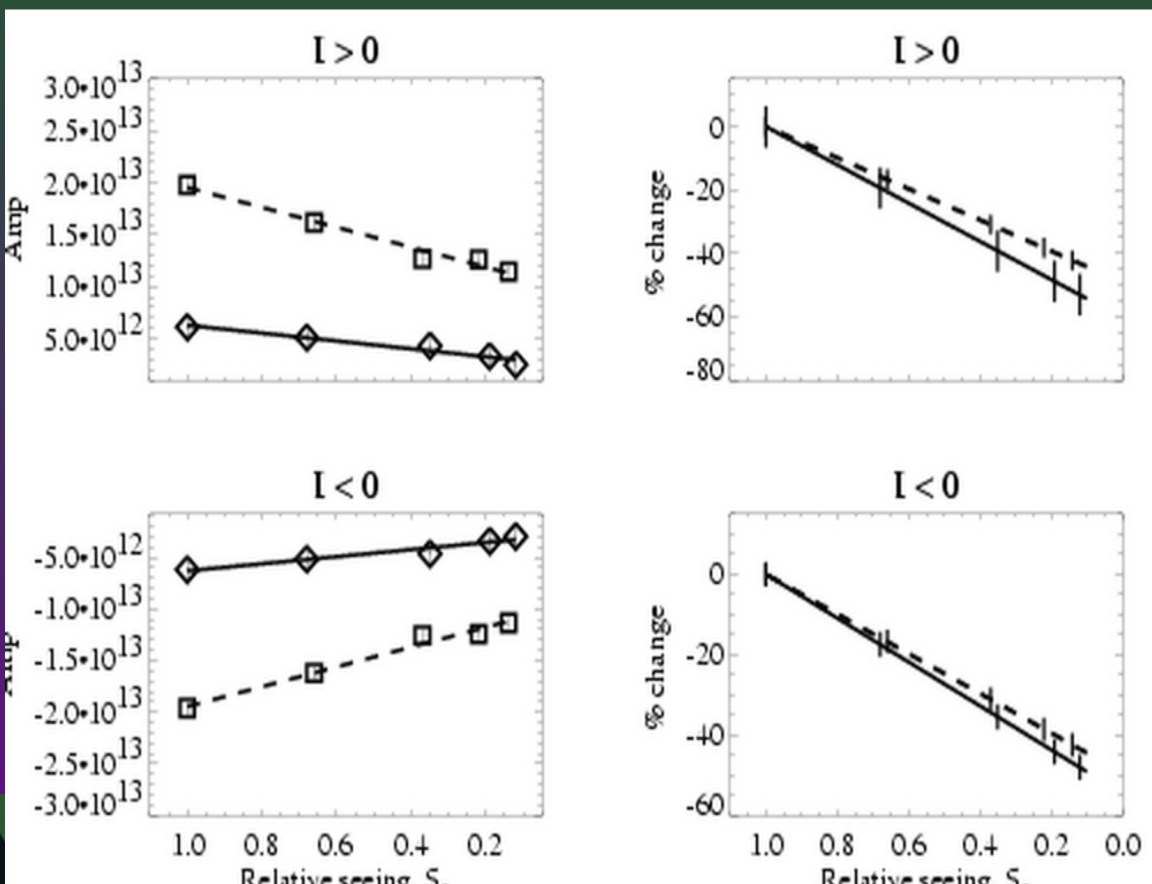

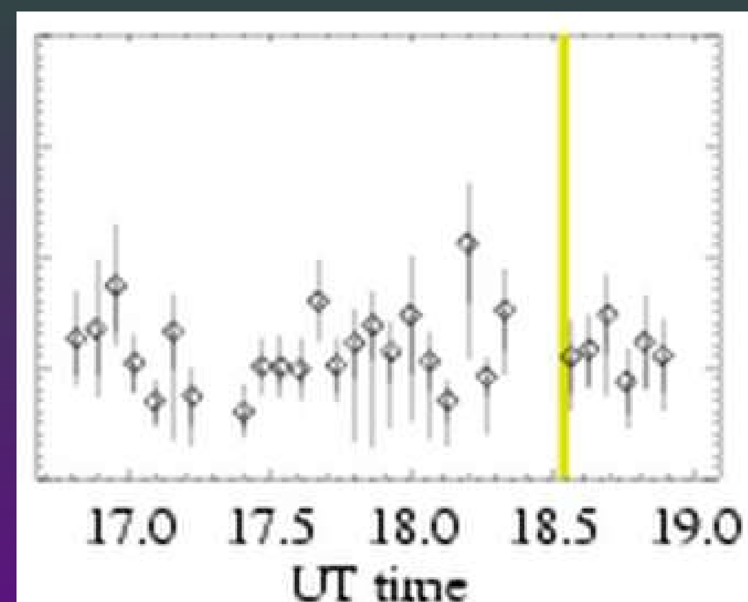

The Data used for this *Demonstration* Study:

- Archived IVM data selected for well-observed flares and flare-quiet (but flare-probable) regions.

- Time sequences divided into *epochs*, each ending with either:
  - a GOES event, or
  - a data-gap, or
  - after more than an hour of continuous data (5-magnetogram min. imposed).

- Final tally: 10 flaring, 14 flare-quiet epochs.

- For each epoch, both the *mean* and *temporal variation* (slope) of the derived parameters are considered.

Table 2: Flaring and Flare-Quiet Epochs

NOAA AR Number	Start Time	End Time	Number Magnetograms	Event
8210	17:07	18:07	20	
8210	18:15	19:14	20	
8210	19:31	20:08	13	C2.8
8210	20:11	21:35	27	C2.6
8210	21:55	22:35	13	M1.2
8210	22:38	23:25	15	
8636	16:47	18:31	23	M1.1
8636	18:35	18:50	5	
8636	19:14	19:30	5	
8636	20:09	20:28	6	
8636	21:04	22:11	14	
8771	18:13	18:38	6	C1.6
8771	18:42	18:58	5	M2.0
8771	19:02	19:34	7	
8891	18:13	19:07	15	
8891	19:43	20:38	15	
8891	20:49	21:24	10	
9026	17:06	18:22	18	C3.8
9026	18:25	18:57	9	
9165	19:44	20:51	17	C7.4
9165	20:55	21:18	7	
0030	18:53	19:58	14	X3.0
0030	20:02	21:02	15	M1.8
0030	22:04	22:24	6	

What can be measured?

Examples:

horizontal gradients

$$|\nabla_h B(x,y)| = \left[\left(\frac{\partial B}{\partial x}\right)^2 + \left(\frac{\partial B}{\partial y}\right)^2\right]^{\frac{1}{2}}$$

vertical current density

$$J_z(x,y) = \frac{C}{\mu_0}\left(\frac{\partial B_y}{\partial x} - \frac{\partial B_x}{\partial y}\right)$$

measures of twist

$$\alpha(x,y) = \frac{[\nabla_h \times \boldsymbol{B}_h]_z}{B_z}$$

current helicity density

$$h_c(x,y) = B_z \cdot [\nabla_h \times \boldsymbol{B}_h]_z$$

magnetic shear angles

$$\Psi(x,y) = \cos^{-1}[\boldsymbol{B}^p \cdot \boldsymbol{B}^o / B^p B^o]$$

$$\psi(x,y) = \cos^{-1}[\boldsymbol{B}_h^p \cdot \boldsymbol{B}_h^o / B_h^p B_h^o]$$

Different parameterizations offer different weighting and sensitivity to measures of magnetic morphology and energy storage.

Images of continuum (top) and Bz (bottom, with +/- 100 G contours) of NOAA AR0030 (left), AR8636 (middle) and AR8891 (right); axes are in Mm. (black triangles are masked field stops).

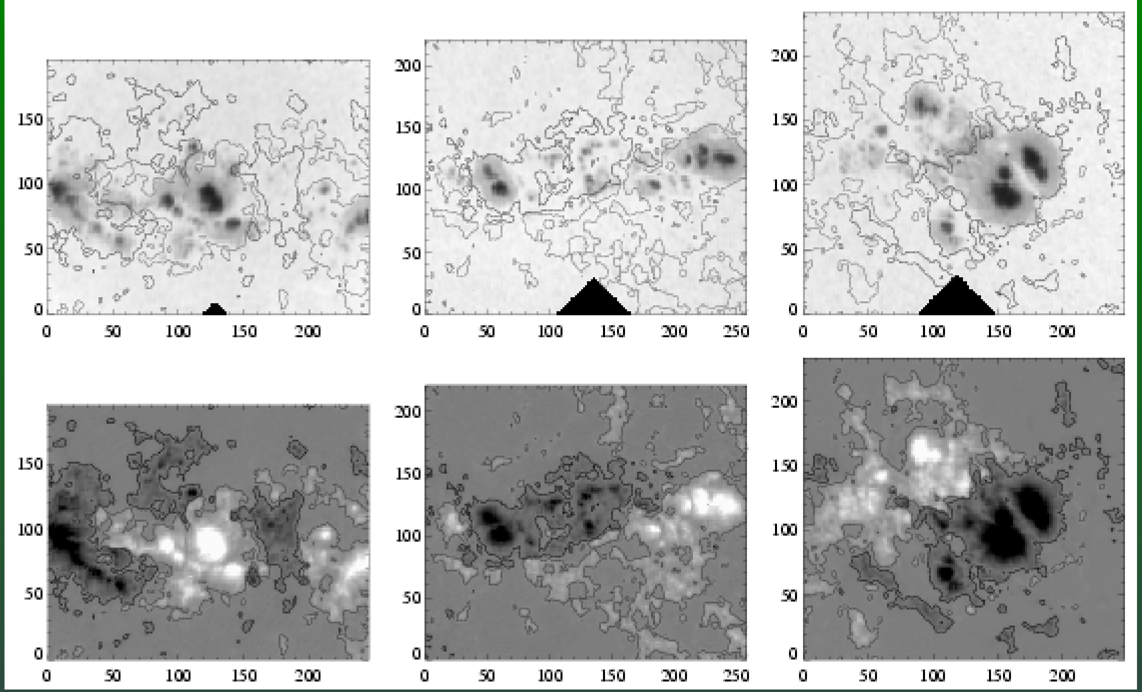

Magnetic state of the photosphere is described by quantities derived from the observed magnetic vector; the spatial distribution is parameterized using the moment analysis:

$$
\begin{aligned}
\text{mean } \overline{x} &= \frac{1}{n}\sum_i x_i \\
\text{standard deviation } \sigma &= \left[\frac{1}{n}\sum_i \left(x_i - \overline{x}\right)^2\right]^{\frac{1}{2}} \\
\text{skew } \varsigma &= \frac{1}{n}\sum_i \left[\frac{x_i - \overline{x}}{\sigma}\right]^3 \\
\text{kurtosis } \kappa &= \frac{1}{n}\sum_i \left[\frac{x_i - \overline{x}}{\sigma}\right]^4 - 3.0
\end{aligned}
$$

(plus summations/means where appropriate)

Goal: identify flare precursors, if any, measurable using photospheric vector magnetic field data.

Example: Magnetic Field Twist

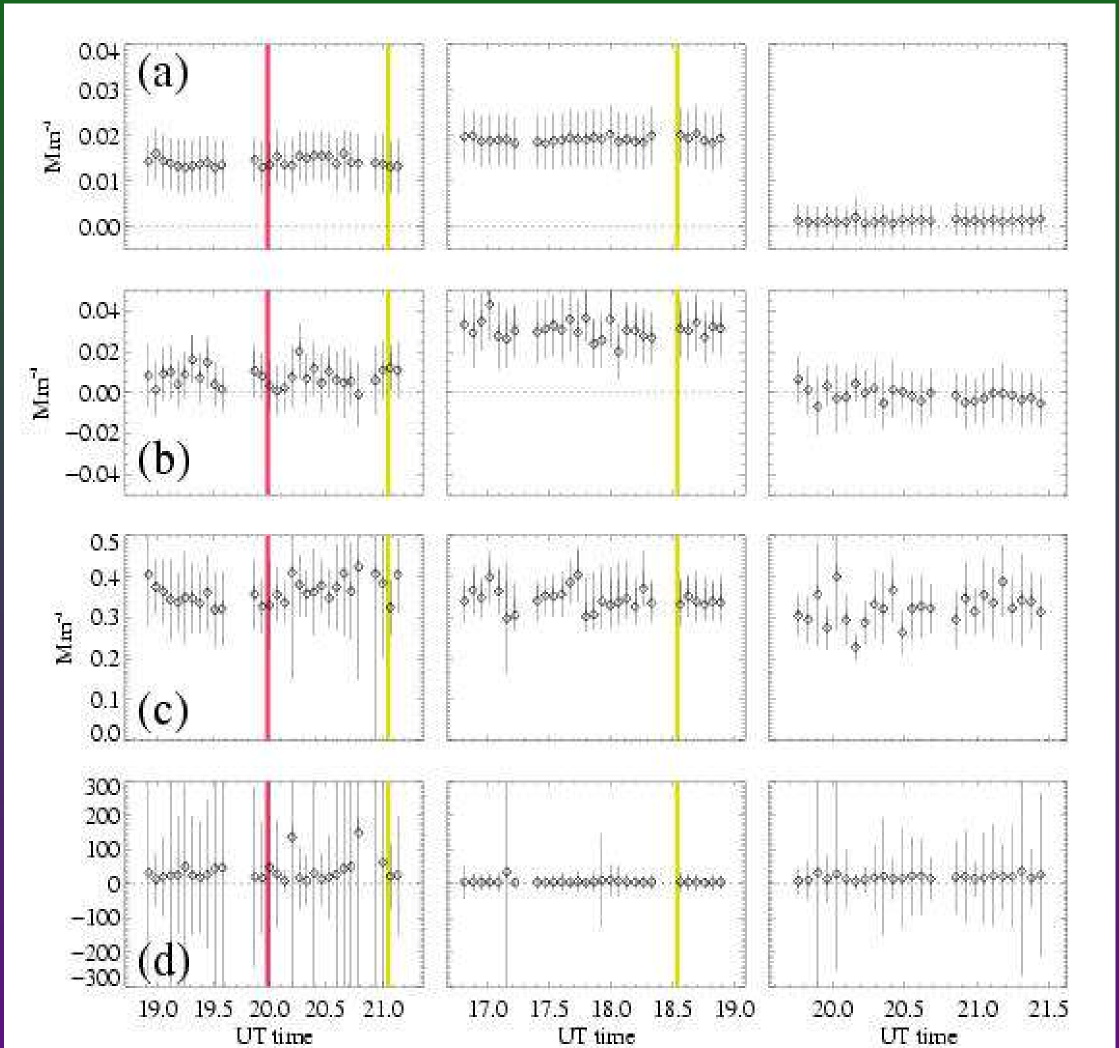

(a) the "best" force-free **α**, fit over entire active region, plotted as a function of time for the three target active regions relative to the start of an **X**- and two **M**-class flares.

(b) the mean of **α**(x,y)

(c) the standard deviation of **α**(x,y)

(d) the kurtosis of **α**(x,y)

Example: Magnetic Shear Angles

Consider four measures:

(a) 3-D shear angle Ψ over entire active region

(b) 3-D shear angle Ψ in NL areas

(c) Horizontal projection of shear angle ψ over entire AR

(d) Horizontal projection of shear angle ψ in NL areas.

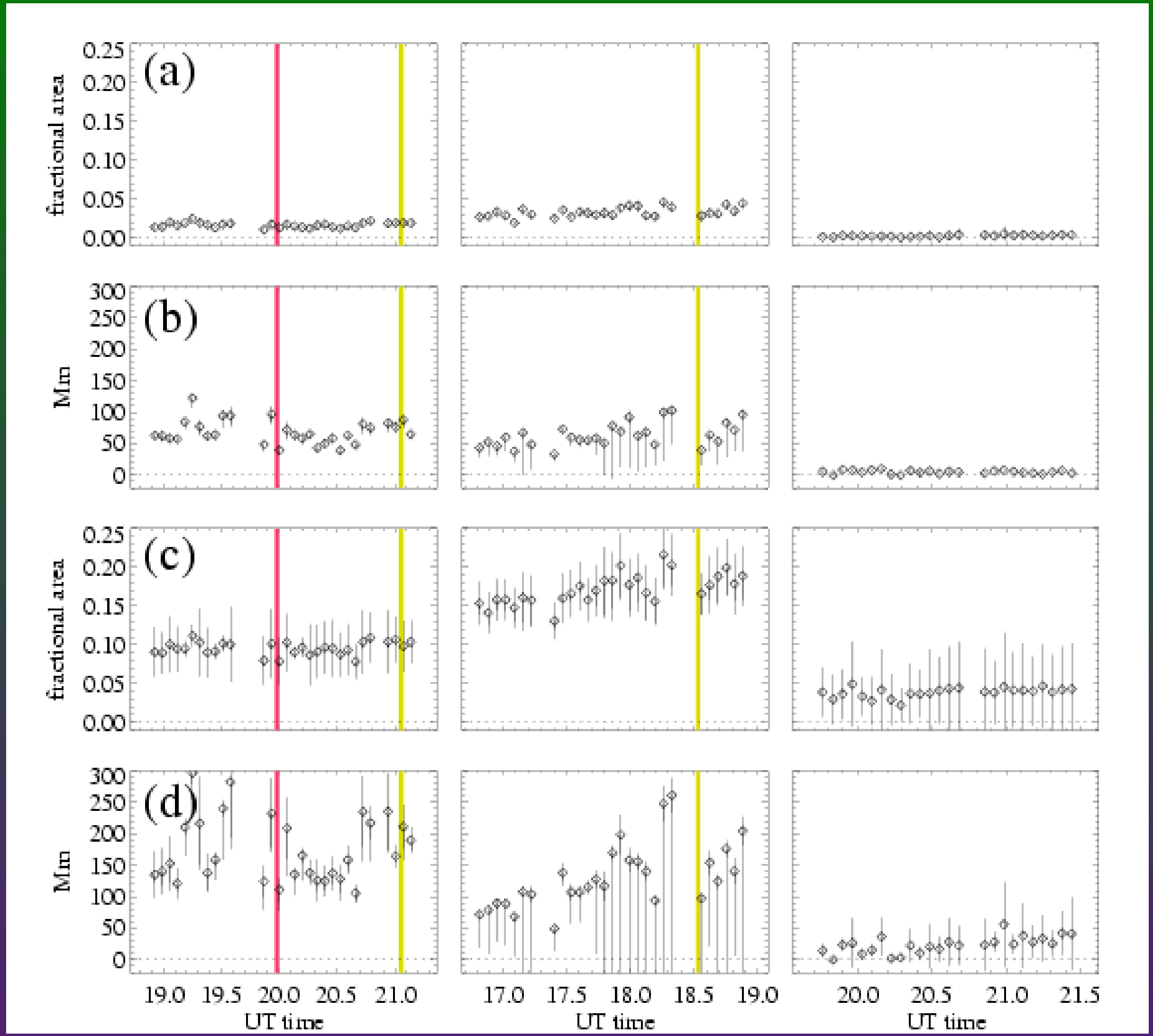

Thus far, little evidence that *any* single measure derivable from photospheric ***B*** implicates a stress/release mechanism in the photosphere.

No single silver bullet

Results from inspection of a gazillion parameters:

- The majority of parameters show inconsistent results. Some display distinct rises/falls prior to flare events when temporal windows are chosen subjectively (e.g., $\kappa(B_h)$, $|\nabla_h B_z|$, $\sigma(J_z)$, $\kappa(J_z)$).
- Relative to flaring epochs, flare-*quiet* epochs show larger $\kappa(\rho_e)$, $\sigma(B_z)$, $\sigma(B_h)$, $|\nabla_h B_z|$ and larger $\sigma(h_c)$, $H_c(tot)$.
- Distinct overall flare-productivity signatures include: larger α_{ff}, greater extent of magnetic shear, larger $H_c(net)$, h_c.
- In most cases, if a parameter exhibits a "significant" rise/fall prior to a flare, it also exhibits similar-magnitude variations during flare-quiet epochs.

Most importantly:

By requiring a flare-unique signature, numerous candidate parameters are *nullified* due to similar behavior during a flare-quiet epoch.

Considering the behavior of a single parameter at a time in this manner can be very informative, but inadequate to determine

"What makes a flare?"

Q: Can samples from two populations (flare-imminent vs. flare-quiet) be distinguished?

Statistical Test #1: Hotelling's T^2 test

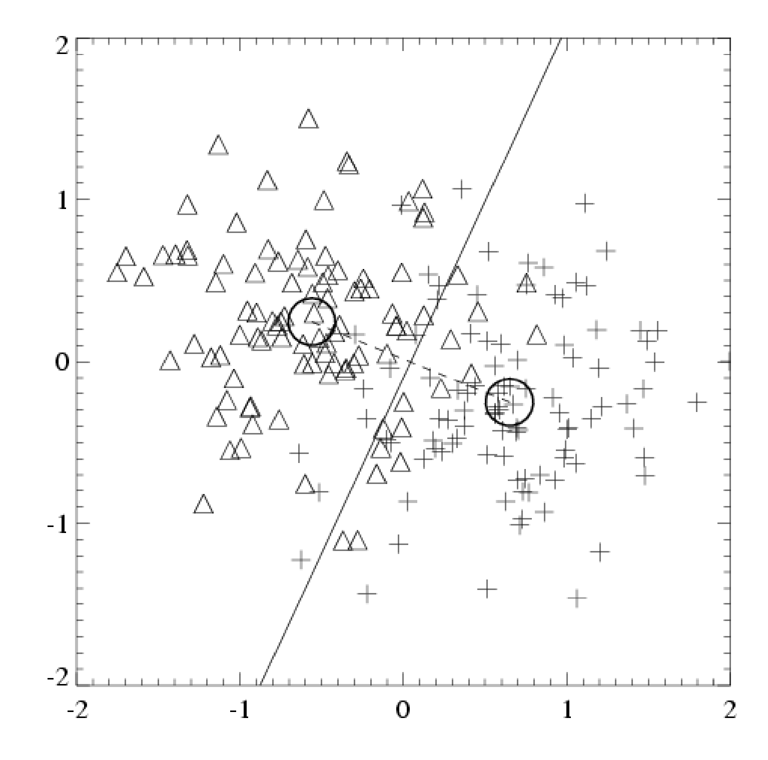

- Gives probability that samples come from distinct populations
- Essentially a measure of the distance between sample means, relative to the sample variance
- Even with a high probability of different parent populations, samples may have a large overlap.
- Simultaneously considers multiple variables.

Statistical Test #2: Discriminant Function Analysis

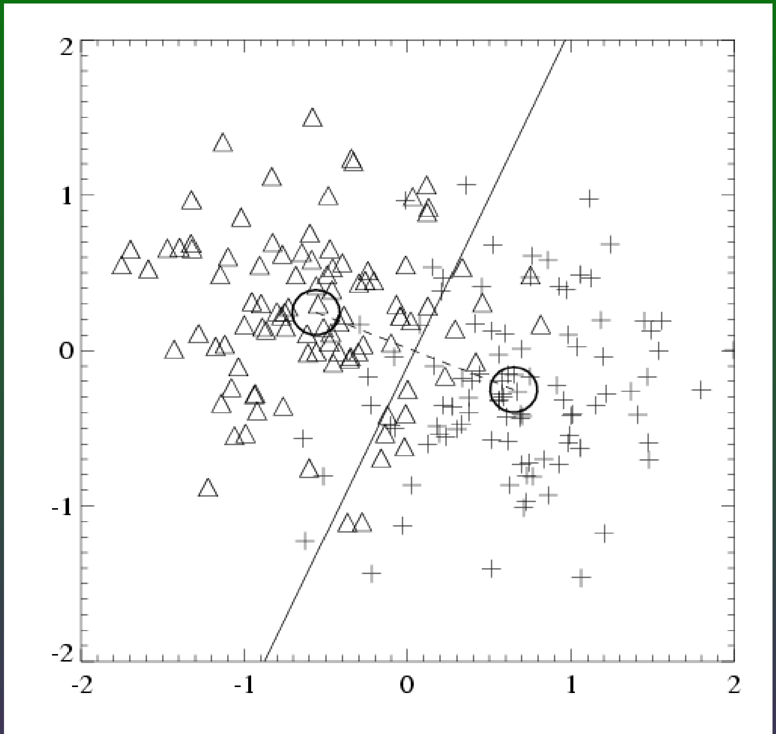

- Given measurements known to originate from two populations, a Discriminant Function divides parameter space into two regions.
- Maximizes correct "prediction" probabilities given equal probabilities for errors of both possible types.
- Simultaneously considers multiple variables.
- Magnitudes of DF coefficients give the relative predictive power of component variables.
- Error rates constructed using "truth tables" or "classification tables"; *these will always underestimate the errors.*
- Unbiased error estimate possible using "n-1" approach.

Gentle Introduction to DFA I:

Total Vertical Current *vs.* Total Magnetic Flux

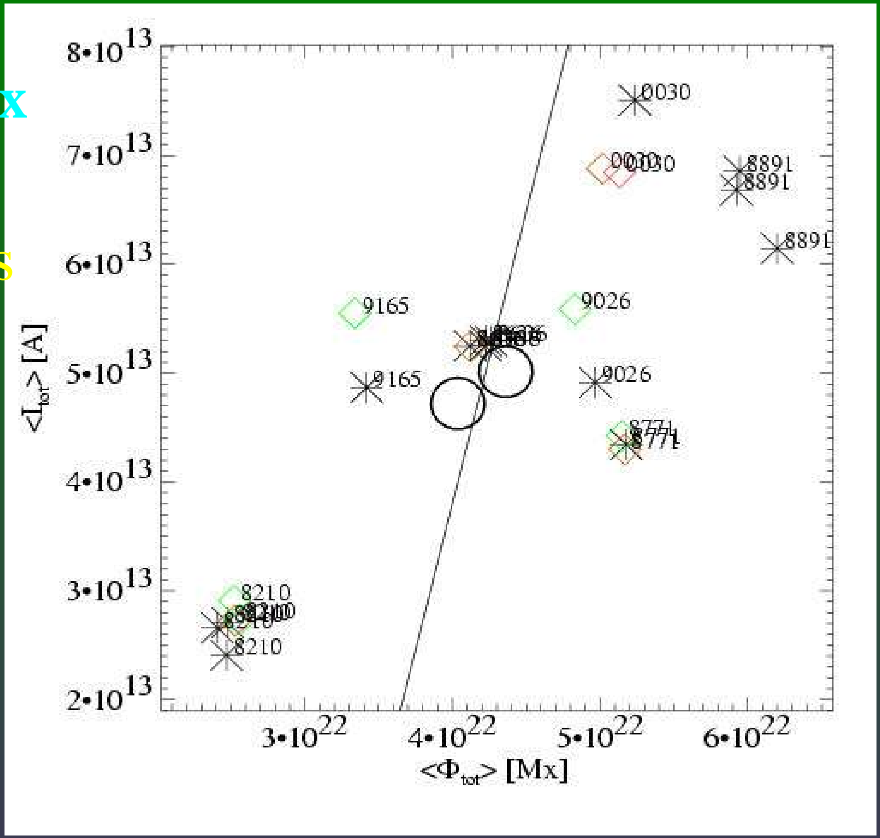

Hotelling's T^2 test: probability that the samples are from different populations: 0.327

Discriminant Function:

$$f = 0.0052 - 0.2891 \langle \Phi_{tot} \rangle + 0.0673 \langle I_{tot} \rangle$$

Classification Table:

		predicted	
		flare	no flare
observed	flare	5	5
	no flare	6	8

Error Rate from table: 0.458

Error estimate from "n-1" approach: 0.625

Parameter space and discriminant function for $[\langle \Phi_{tot} \rangle, \langle I_{tot} \rangle]$; ◇: flaring epochs with [C, M, X]-class flares. ✳: quiet epochs. ○: means of each sample. Solid line: discriminant function. Variables are correlated (although not related), which reduces the DF's usefulness as a comparative prediction tool, and results in a non-perpendicular angle between it and the line connecting the two sample means.

Gentle Introduction to DFA II:

Temporal variation of the kurtosis of the twist distribution *vs.* temporal variation of the standard deviation of the inclination angle distribution.

Hotelling's T^2 test: probability that the samples are from different populations: 0.943

Discriminant Function:

$f = 0.115 - 1.312\, d\sigma(\gamma)/dt + 1.434\, d\kappa(\alpha)/dt$

Classification Table:

		predicted	
		flare	no flare
observed	flare	8	2
	no flare	4	10

Error Rate from truth table: 0.250

Error estimate from "n-1" approach: 0.250

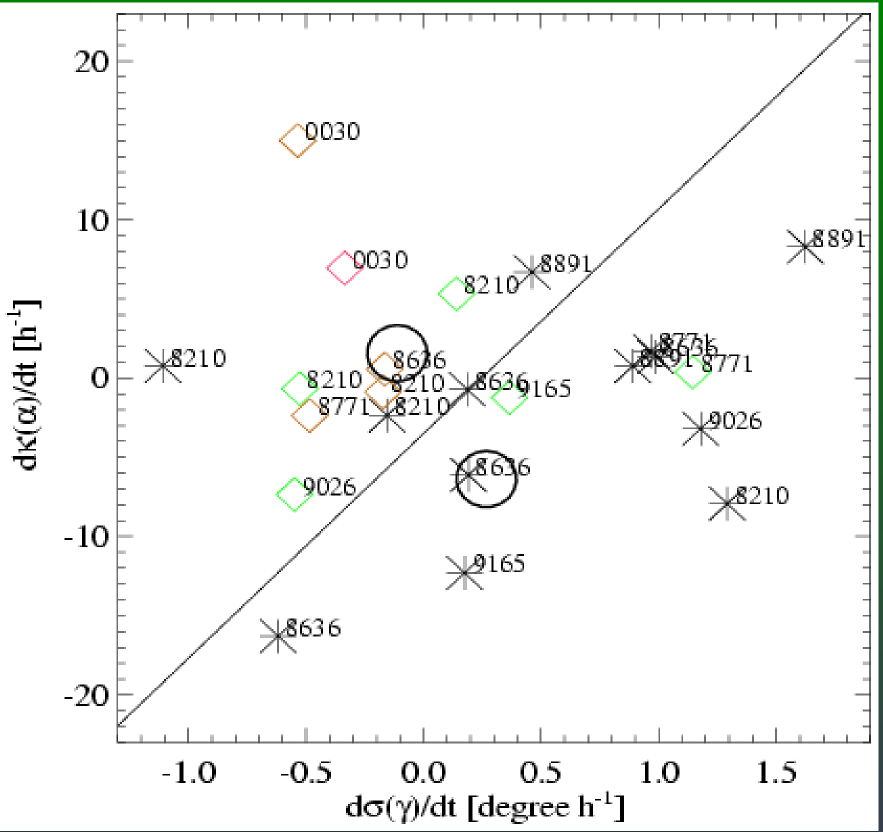

Parameter space and discriminant function for [dσ(γ)/dt, dκ(α)/dt]. ◇: flaring epochs with [C, M, X]-class flares. ✳: quiet epochs. ○: means of each sample. Solid line: discriminant function. Variables are not correlated, which results in a DF perpendicular to the two sample means.

Fully Exploiting the Data and Analysis: Discriminant Functions of more than two variables

- **DF becomes a hyper-plane in parameter-space**
- **Still small-number statistics: *results here are for demonstration only!***

Example: Two Two-variable DFs:

$f\,[\,\langle\sigma(\psi)\rangle, \langle\kappa(hc)\rangle\,]$, probability $= 0.047$

$f\,[\,\langle\sigma(Bh)\rangle, \langle\kappa(|\nabla Bh|)\rangle\,]$, probability $= 0.625$

Combine for a four-variable DF:

$$f = 0.327 - 8.574\,\langle\sigma(\psi)\rangle - 2.277\,\langle\kappa(hc)\rangle - 5.690\,\langle\sigma(Bh)\rangle + 7.479\,\langle\kappa(|\nabla Bh|)\rangle$$

Hotelling's T^2 probability: **0.997**

Classification Table:

		predicted	
		flare	no flare
observed	flare	8	2
	no flare	2	12

Error Rate from table: **0.167**

Error estimate from "n-1" approach: **0.292**

Example: Six-Variable Discriminant Function:

$$\begin{aligned} f &= 1.021 - 11.098\,\langle \sigma(B_h)\rangle + 7.460\, d\overline{B_z}/dt + 8.330\,\langle \varsigma(J_z^h)\rangle - 3.829\,\langle \kappa(J_z^h)\rangle \\ &- 7.718\,\langle A(\psi > 80^\circ)\rangle - 3.834\, d|\alpha_{ff}|/dt \end{aligned}$$

Hotelling's T^2 probability: **0.999995**

Classification Table:

		predicted	
		flare	no flare
observed	flare	10	0
	no flare	0	14

Error rate from table: **0.00**
Error estimate from "n-1" approach: **0.125**

Perfect classification is possible with the data and variables considered here. This example is *not unique*: there are many other combinations which result in perfect classification tables and Hotelling T^2 probabilities *above* 0.999990.

Q: Which parameters are most strongly associated with flaring?

Ideal World: Construct a single discriminant function and evaluate all variables simultaneously.

Real World: small number statistics still preclude this.

Proxy: “the probability sort”:

- *Every combination* for a given number of variables is considered.
- *Each* is evaluated and the *results sorted* according to the Hotelling's T^2 probability.
- *Example*: consider single variables, and the results of their probability sort:
  - Highest probability for a single variable that a flaring/non-flaring atmosphere can be distinguished is only 0.703, and from a non-robust variable at that.
  - Confirmation of the inconsistent flare-prediction results considering one variable at a time.

1-Variable	
Variable	Probability
$d\lvert\Phi_{net}\rvert/dt$	0.703
$\langle\lvert\Phi_{net}\rvert\rangle$	0.673
$d\varsigma(h_c)/dt$	0.671
$\langle L(\Psi_{NL} > 80^\circ)\rangle$	0.668
$d\kappa(\alpha)/dt$	0.656
$d\overline{\psi_{NL}}/dt$	0.636
$\langle\varsigma(h_c)\rangle$	0.636
$d\Psi_{NL}/dt$	0.631
$\langle\sigma(B_h)\rangle$	0.624
dI_{tot}/dt	0.614
$d\lvert I^h_{net}\rvert/dt$	0.610
$d\Psi/dt$	0.608
dI^h_{tot}/dt	0.588
$\langle\sigma(\alpha)\rangle$	0.587
$\langle\sigma(\lvert\nabla_h B_h\rvert)\rangle$	0.585
$\langle B_h\rangle$	0.561
dJ^h_z/dt	0.557
$\langle\lvert\nabla_h B_h\rvert\rangle$	0.556
$d\sigma(B_h)/dt$	0.554
$d\kappa(B_z)/dt$	0.549

Four-Variable sort:

4-Variable	
Variable	Frequency
$d\kappa(\alpha)/dt$	244
$\langle\sigma(\alpha)\rangle$	209
$\langle\kappa(B_h)\rangle$	164
$\langle\sigma(B_h)\rangle$	158
$\langle\sigma(\psi)\rangle$	79
$\langle\lvert\Phi_{net}\rvert\rangle$	71
$d\sigma(\gamma)/dt$	59
$\langle\kappa(\lvert\nabla_h B_h\rvert)\rangle$	58
$d\kappa(\gamma)/dt$	47
$\langle\varsigma(\lvert\nabla_h B_h\rvert)\rangle$	46
$d\overline{J_z^h}/dt$	27
$dA(\Psi > 45°)/dt$	27
$d\overline{B_z}/dt$	25
$\langle L(\Psi_{NL} > 80°)\rangle$	25
$dA(\psi > 45°)/dt$	24
$\langle\varsigma(J_z^h)\rangle$	22
$\langle\overline{\psi_{NL}}\rangle$	21
$d\overline{\Psi_{NL}}/dt$	20
$d\sigma(B_h)/dt$	20
$d\varsigma(h_c)/dt$	18

The distribution of probabilities for all 4-variable combinations containing (a) ⟨σ(Bh)⟩, and (b) ⟨σ(ψ)⟩. Both occur with high frequency in the best combinations from the probability sort, but their "parents" display quite different probability distributions.

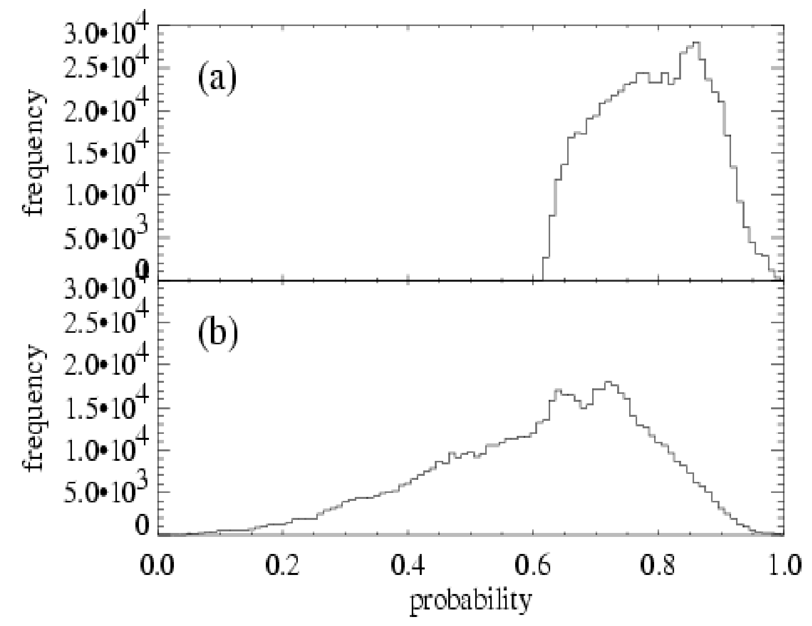

Test the Proxy: a 10-variable Discriminant Function

- Compare the variables' standardized coefficients with their frequency in best and worst 4-variable combinations.

- Validation of probability sort method as proxy for constructing larger Discriminant Functions.

Ten Variable Discriminant Function Coefficients

Variable	Standardized Coefficient	Frequency in Best	Frequency in Worst
$d\kappa(\alpha)/dt$	2.444	244	0
$\langle\sigma(\alpha)\rangle$	1.964	209	0
$\langle\kappa(B_h)\rangle$	1.575	158	0
$\langle\sigma(B_h)\rangle$	-1.326	79	0
$\langle\sigma(\psi)\rangle$	-0.520	164	152
$d\sigma(\rho_e)/dt$	0.492	1	154
$\langle\overline{B_z}\rangle$	-0.370	5	178
$dA(\Psi > 80°)/dt$	0.352	6	188
$d\overline{B_h}/dt$	-0.258	2	187
$\langle\kappa(\Psi)\rangle$	0.204	3	176

Summary.....

- Examining time-series magnetic field data for changes in single parameters relative to flare occurances can be an informative first step.
- By ensuring a flare-unique signature, however, numerous candidate parameters (considering both their variation and overall magnitude) are nullified on account of similar behavior in a flare-quiet region.
- A statistical approach is required to quantitatively evaluate parameters with respect to flare prediction; we demonstrate the application of Discriminant Function Analysis and Hotelling's T^2 statistic.
- Parameter-combinations can be found which result in quite good predictions, however...
  - The combinations are not unique and hence larger numbers of variables must be considered simultaneously.
  - The large number of variables considered coupled with a small data set is likely to result in spurious perfect classification tables.
- A full implementation to obtain physically meaningful results requires much more data.
- **We demonstrate here the requisite approach: include flare-quiet epochs as a control group for statistical tests of the null hypothesis.**

Quantifying the coronal magnetic complexity: Magnetic Charge Topology

(Barnes, Longcope & Leka, in preparation)

- Model the coronal magnetic field above an active region as due to a collection of point sources.
- Compute the magnetic flux in each magnetic connection
- Locate magnetic null points, separator field lines
- Use the topological properties to quantify the coronal complexity

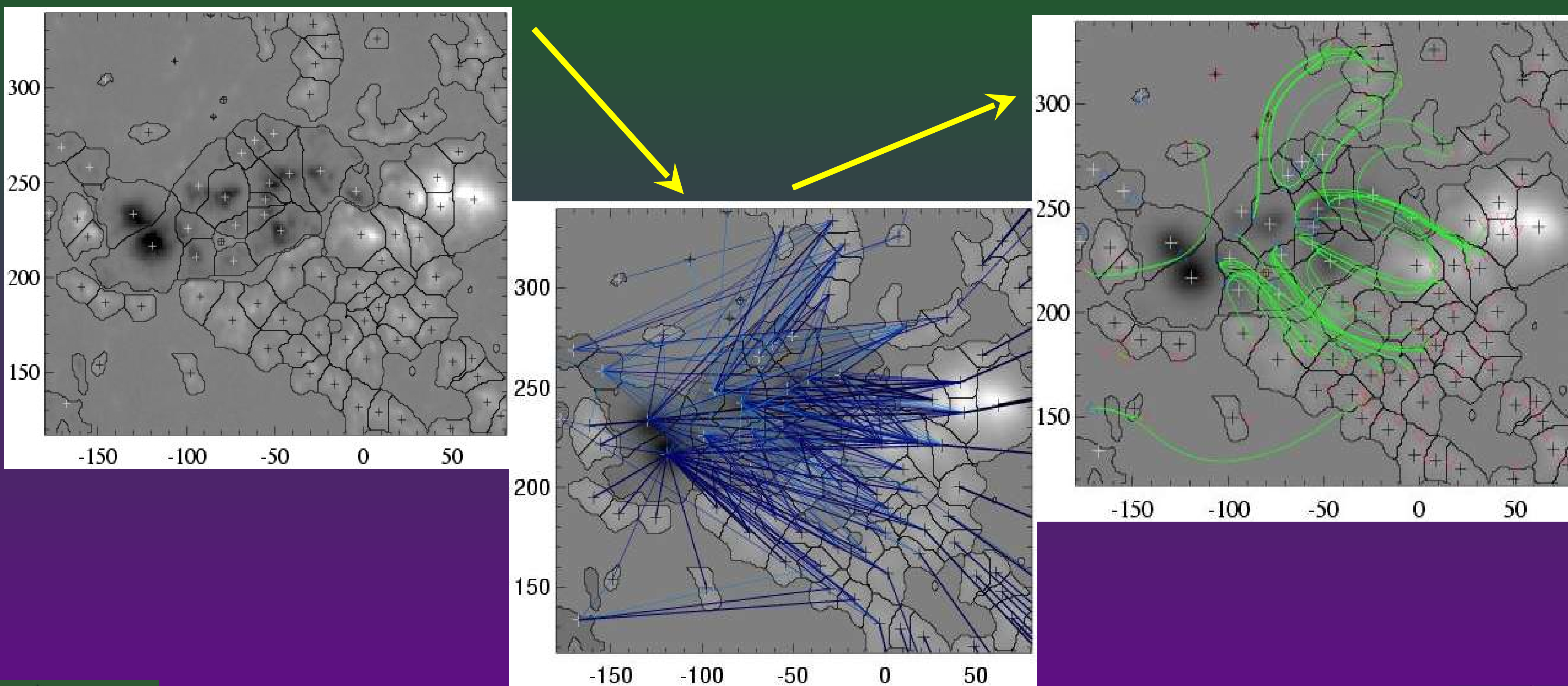

Parameterizations of Coronal Complexity

Magnetostatic energy:
may measure the resevoir of available energy.

$$E_B = \sum_{i<j} \frac{q_i q_j}{|\boldsymbol{x}_i - \boldsymbol{x}_j|}$$

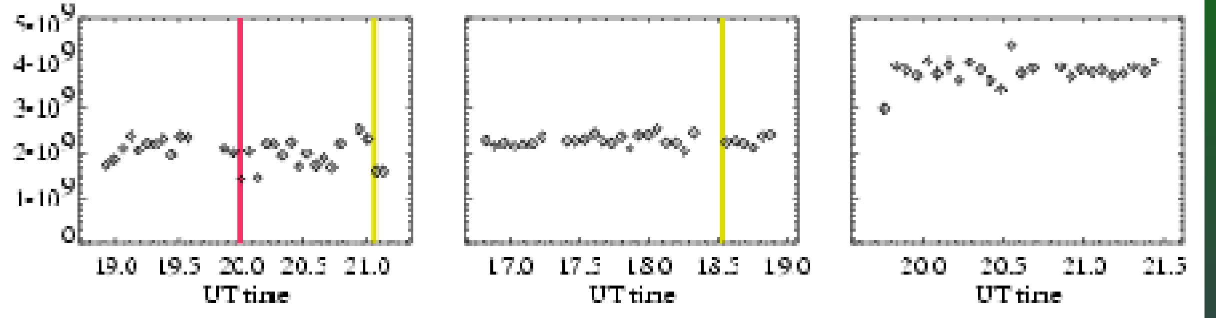

Number of Separators:
quantifies magnetic complexity and possible locations for magnetic reconnection.

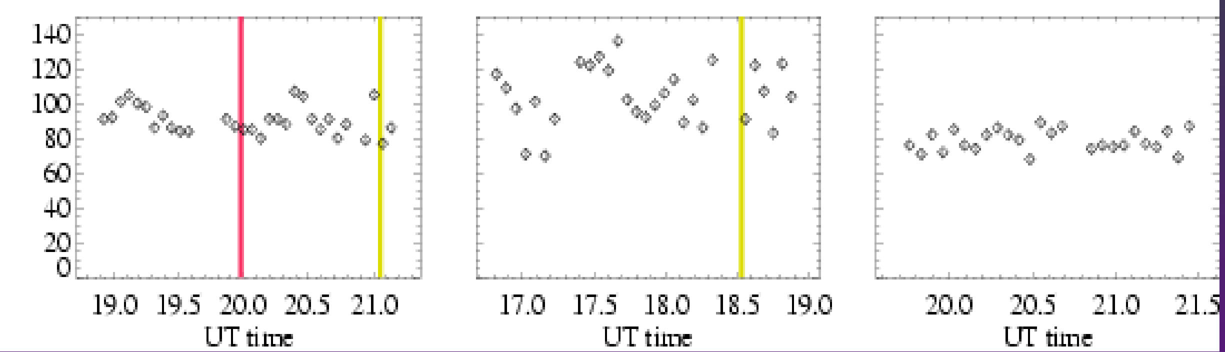

Applying Discriminant Function Analysis to Coronal Complexity Parameterizations

Example: 6-variable DF:

$$f = 0.56 + 2.97\langle n_{sep}\rangle - 2.77\langle E_B\rangle + 8.06\frac{d\sigma(q)}{dt} - 8.34\frac{d\kappa(q)}{dt} - 8.41\frac{d\sigma(\varphi)}{dt} - 10.13\frac{d\kappa(\xi)}{dt}$$

Hotelling's T^2 probability: **0.99978**

Classification Table:

		predicted	
		flare	no flare
observed	flare	10	0
	no flare	0	14

Error rate from table: **0.00**

Error estimate from "n-1" approach: **0.083**

Summary:

- Examining the coronal magnetic field topology for flare productivity and prediction makes sense physically; MCT is one way to approach it.
- Resulting parameterizations can be examined statistically; results from this demonstration are promising as well with similar caveats as earlier.

Future Projects Include:

- Incorporate additional photospheric data (in progress).
- Explore unequal cost/benefit capability of DF analysis.
- Apply full analysis to chromospheric magnetic field data (acquisition is now standard with the IVM; database is building).
- Apply full analysis to simulated active region data (Fan & Gibson) to investigate:
  - Whether model data show different pre-eruptive signatures than observed data, and to
  - Use results from observed data to refine the model construct.